

A phase separation of active colloidal suspension via Quorum-sensing

Francis Jose,^{1,*} Shalabh K. Anand,^{1,†} and Sunil P. Singh^{1,‡}

¹*Department of Physics,
Indian Institute of Science Education and Research,
Bhopal 462 066, Madhya Pradesh, India*

We present the Brownian dynamics simulation of active colloidal suspension in two dimensions, where the self-propulsion speed of a colloid is regulated according to the local density sensed by it. The role of concentration-dependent motility on the phase-separation of colloids and their dynamics is investigated in detail. Interestingly, the system phase separates at a very low packing fraction ($\Phi \approx 0.125$) at higher self-propulsion speeds (Pe), which coexists with a homogeneous phase and attains long-range crystalline order beyond a transition point. The transition point is quantified here from the local density profiles, local and global-bond order parameters. We have shown that the phase diagram's characteristics are qualitatively akin to the active Brownian particle (ABP) model. Moreover, our investigation reveals that the density-dependent motility amplifies the slow-down of the directed speed, which facilitates phase-separation even at low packing fractions. The effective diffusivity shows a crossover from quadratic rise to a power-law behavior of exponent $3/2$ with Pe in the phase-separated regime. Furthermore, we have shown that the effective diffusion decreases exponentially with packing fraction in the phase-separated regime while linear decrease in the single phase regime.

PACS numbers:

I. INTRODUCTION

A collection of self-propelled units constitutes an out-of-equilibrium system that harvests ambient energy from the environment to perform a long-persistent motion [1–3]. These systems exhibit complex collective dynamics which are markedly different from their passive counterpart, such as self-organisation at low density [4–11], flocking [12, 13], swarming [14], vortex-formation [15], the formation of linear chains [16], anomalously large density fluctuations [17], non-monotonic behavior in the active pressure [18–20], etc. In the past, phase separation of the self-propelled systems has been rigorously explored in the laboratories where dynamical structures are contrived by employing light controlled motion of active colloids [15, 21, 22], diffusiophoretic motion or concentration-gradient driven motion [22–28].

Within the framework of theory and simulations, the phase-separation of a self-propelled system of hard colloids has been explored by treating their motion either as a ‘run and tumble’ model [29–32], active Ornstein-Uhlenbeck (AOU) particles [33–35], or as an active Brownian particle (ABP) model [36–45]. The self-propulsion causes phase separation referred as motility-induced phase separation (MIPS) [17, 43, 46–57], which is a consequence of the slow-down of the active colloids produced by steric-interactions [57, 58]. In MIPS, a liquid-like dense aggregate of slow-moving colloids coexists with a gas-like phase of fast-moving colloids at low-

density [17, 43, 46–55, 57]. In the standard ABP model, the phase-separation arises at packing fractions ($\Phi = 0.4$) even in the absence of any attractive or alignment interactions [17]. Additionally, the presence of an attractive short-range interaction among ABPs causes significant changes on local inhomogeneity, separation of mixtures, and also adds to re-entrant phase behavior [11, 59].

The aggregation in biological systems at low density is a ubiquitous phenomenon [60–62]. Concurrently, coordinated motion in these systems is often a consequence of complex communication pathways among their individual units. Bacterial colonies, like *Aliivibrio fischeri*, *Vibrio harveyi*, *Erwinia carotovora*, etc., produce extracellular enzymes called auto-inducers, which regulate their gene expression [63–68], thus act as a means of communication among cells [67, 69]. For instance, *Aliivibrio fischeri* [65] produces luminescence after their local population growth surpasses a threshold density. The communication among the bacterial cells triggered by the variation in local population density is termed ‘quorum-sensing’. It plays vital role in the regulation of various physiological processes like manoeuvring local population density, regulation of gene expression [65–67], communication among cells [67, 69], motility [66, 69], etc. Despite the vast applications of ‘quorum-sensing’ in biology, this subject has been addressed far less in simulations, especially for the ABPs [42, 57, 70].

The variation of self-propulsion speed as a function of local density has been accounted in theoretical continuum models using phenomenological hydrodynamic equations with local density as a coarse-grained field. Interestingly, this model also unveils MIPS. Importantly, it provides a unified approach for the phase-separation using quorum-sensing rule and the generic constant activity model with pair-wise interactions [47, 57, 71]. A detailed study on

*Electronic address: francisjm24@gmail.com

†Electronic address: skanand@iiserb.ac.in

‡Electronic address: spsingh@iiserb.ac.in

the role of controlled and explicit density-dependent activity on the MIPS would provide more insights into the underlining behavior. We attempt here to reveal the role of quorum-sensing contribution along with pair-wise repulsive forces in the phase separation. Additionally, we compare our results to that of generic ABP model.

The article presents Brownian dynamics simulation of ABPs whose motility is regulated by linearly decreasing self-propulsion force with local density. The density-dependent motility induces cluster formation with hexatic ordering at relatively low packing fractions $\Phi \geq 0.125$, in the high activity regime. The local density distribution confirms the presence of large dense clustered phase coexisting with a homogeneous low-density phase beyond a critical density. The local and global order parameters such as Ψ_6 and C_{q6} , respectively, ascertain the presence of hexatic ordering at higher Péclet numbers. We have shown that the emergence of the coexistence of low and high-density phases at very low packing is a consequence of multi-body collisions leading to drastic slow-down of the swim speed. In addition, the effective diffusion coefficient in the phase-separated state displays a cross over from a parabolic rise to a power-law behavior with an exponent $3/2$ with Péclet number [18, 20]. Moreover, the total pressure exhibits a sharp decrease in the phase-separated regime, as expected.

The article is organised as follows: Section 2 elaborates the simulation approach, all the results are presented in section 3 that consists 5 different sub-sections, with the summary in section 4.

II. SIMULATION MODEL

We model self-propelled discs, in two dimensions, interacting with each other via repulsive-shifted Lennard Jones (LJ) potential,

$$U_{LJ}(r_{ij}) = \begin{cases} 4\epsilon \left[\left(\frac{\sigma}{r_{ij}} \right)^{12} - \left(\frac{\sigma}{r_{ij}} \right)^6 \right] + \epsilon, & r_{ij} \leq 2^{1/6}\sigma, \\ 0, & r_{ij} > 2^{1/6}\sigma. \end{cases} \quad (1)$$

Where $r_{ij} = |\mathbf{r}_i - \mathbf{r}_j|$ is the distance between the pair i and j , ϵ is the LJ energy, and σ is the diameter of disc.

The equation of motion for the position and its orientation vector are governed by the over-damped Langevin equation,

$$\begin{aligned} \dot{\mathbf{r}}_i &= \frac{1}{\gamma} \left[- \sum_{j=1}^{N_m} \nabla_i U_{LJ}(r_{ij}) + F'_{a,i} \hat{\mathbf{e}}_i + \mathbf{F}_i^R \right], \\ \dot{\theta}_i &= F_i^\theta. \end{aligned} \quad (2)$$

Where γ is the drag coefficient, F_i^R is the thermal noise with zero mean, $F'_{a,i}$ is the magnitude of the active force, and its orientation is given by the unit vector $\hat{\mathbf{e}}_i = (\cos \theta_i, \sin \theta_i)$. The direction of polar vector $\hat{\mathbf{e}}$ obeys

the equation of motion of rotational diffusion, angle θ_i measured from the x-axis.

The friction coefficient and the thermal noise are coupled via fluctuation-dissipation relation, $\langle F_{i\alpha}^R(t) F_{j\beta}^R(t') \rangle = 2\gamma \delta_{\alpha,\beta} \delta_{ij} k_B T \delta(t - t')$. Similarly, F_i^θ is a random torque on a particle, and the relation of random torque with rotational diffusion is given as $\langle F_i^\theta(t) F_j^\theta(t') \rangle = 2D_R \delta(t - t') \delta_{ij}$. Where, $D_t = k_B T / \gamma$ and $D_R = 3D_t / \sigma^2$ are the translational and rotational diffusion constants, respectively.

The effect of local environment on the motility is taken in an approximate manner. For simplicity, motility ($F'_{a,i}$) of a particle is assumed to be a linear function of its nearest neighbors within a fixed cut-off distance, $R_c \leq 1.3$. Thus the active force linearly diminishes with the increase in local population as,

$$F'_{a,i} = \begin{cases} F_{a,i}, & n \leq 2, \\ \beta F_{a,i} \left(\alpha - \frac{\phi_i}{\phi_m} \right), & 2 < n \leq 6, \end{cases} \quad (3)$$

and $F'_{a,i} = 0$ for $n > 6$, where n stands for the number of nearest neighbors of the i^{th} particle, $F_{a,i}$ is the active force on an isolated particle that is modified to $F'_{a,i}$ in the presence of neighbors within a cut-off distance of $R_c = 1.3\sigma$. Here, R_c is chosen approximately to the first minimum in the radial distribution function of a dense system. The cut-off is chosen larger than the pair-wise interaction potential.

The constants $\alpha = 1$ and $\beta \approx 1.8$ are chosen so that the function is calibrated in a linearly decreasing form from $F'_{a,i} = F_{a,i}$ to 0. If the center of a neighboring particle crosses the cut-off distance, then it is assumed to be completely inside the screening area. The apparent local area fraction of the circle of radius R_c within the n neighbors of particle i and itself at the center is approximated as $\phi_i = \lambda [\pi(\frac{\sigma}{2})^2 + n\mathcal{A}]$, with $\lambda = (\pi R_c^2)^{-1}$, $\mathcal{A} \approx 0.6531\sigma^2$ is the approximate maximum area of the neighboring disk to i located within the cut-off distance R_c , $\phi_m = \lambda [\pi(\frac{\sigma}{2})^2 + n\mathcal{A}]$ which is same as ϕ_i at $n = 6$.

The parameters are presented in the dimensionless form with the length scaled by σ , energy in the unit of $k_B T$ (thermal energy), and time in unit of $\tau = \sigma^2 / D_t$. The Brownian dynamics simulation is employed with a time step in the range of $10^{-4}\tau$ to $10^{-5}\tau$. The simulation box is taken to be a square with a side of length L and periodic in each direction. All the results are quantified in the parameter landscape of packing fraction $\Phi = \pi\sigma^2 N / 4L^2$, and dimensionless Péclet number $Pe = F_a \sigma / k_B T$ in equivalence with self-propulsion speed. The number of particles $N = 5041$, unless stated otherwise. The box length L is varied to achieve the packing fractions 0.05 to 0.4 and Pe is varied in the range of 0 to 250. The good statistics for each simulation data set is generated by averaging over ten independent ensembles.

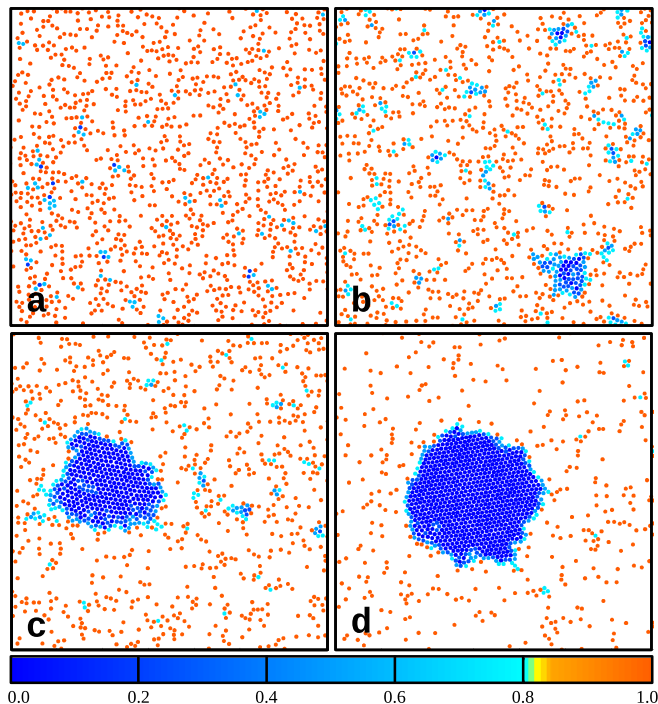


FIG. 1: A set of snapshots corresponding to various Péclet numbers, a) $Pe = 5$, b) $Pe = 50$, c) $Pe = 60$, and d) $Pe = 200$ at $\Phi = 0.20$, $N = 1225$. The particles are color-coded according to their fraction of self-propulsion force $F'_{a,i}/F_{a,i}$. The color gradient denotes the relative speed of the particles from fast motion (red) to slow motion (blue).

III. RESULTS

A. Phase Separation

The considered system of quorum sensing ABPs is observed to display phase-separation at a high activity strength even at very low densities. The simulation snapshots in Fig. 1- a, b, c, and d, at $Pe = 5$, 50, 60, and 200 respectively, illustrate the emergence of the aggregated-dense structures. For low Péclet numbers, the system exhibits mostly gas-like homogeneity, with a few small aggregates having a short life-time. These aggregates grow in the intermediate regime ($5 < Pe < 50$ for $\Phi = 0.2$) with liquid-like characteristics (see Fig. 1-a and b). However, the dense aggregate grows further for large Pe and remains stable for all time scales. The size of the largest aggregate attains the order of the system size in the asymptotic limit $Pe \gg 50$ for $\Phi = 0.2$ (see Fig. 1-d). Moreover, once in the steady-state at high Péclet numbers, the aggregate acquires a long-range ordering, as Fig. 1-c and d illustrate, concurrent with the previous studies [17, 43].

The phase separation in ABPs is a consequence of multi-body collisions at large Pe causing slow-down of the speed in the denser region, which further leads to the aggregation of slow-moving colloids. Figure 1 illustrates

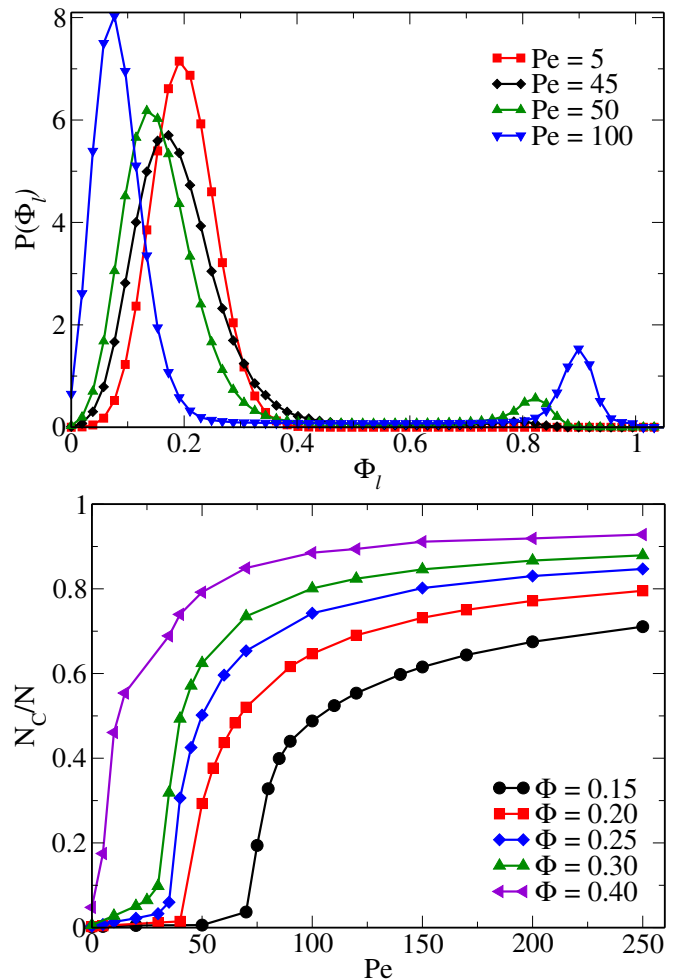


FIG. 2: a) The probability distribution $P(\Phi_l)$ of the local packing fractions plotted for various Pe at given $\Phi = 0.2$. The curve becomes bimodal at the transition point $Pe \approx 45$ depicting the presence of a dense clustered region. b) The average fractional size of the largest cluster N_C/N (N_C is average size of the largest cluster), with Pe for various packing fractions (Φ) in the range of 0.15 to 0.4.

this effect, where blue color represents slow-moving colloids while the reds are fast-moving. The chosen model for density-dependent motility imparts influence on microscopic dynamics. Hence, it is imperative to examine the structural properties from a microscopic perspective. For that, we probe the heterogeneous local density profiles appearing at large Pe . In order to compute the normalised local density profile (Fig.2-a), the simulation box is divided into smaller subsystems (6×6), which is approximately 500 times smaller than the original system. The local packing fraction Φ_l is estimated in these subsystems at $\Phi = 0.2$. In the large Pe limit ($Pe \geq 50$ for $\Phi = 0.2$), the normalised density distribution displays a bimodal peak, one at a lower density and the other at higher density (aggregated phase). The characteristic feature of phase-separation, i.e. coexistence of low and high density phases, is distinctly captured in the local

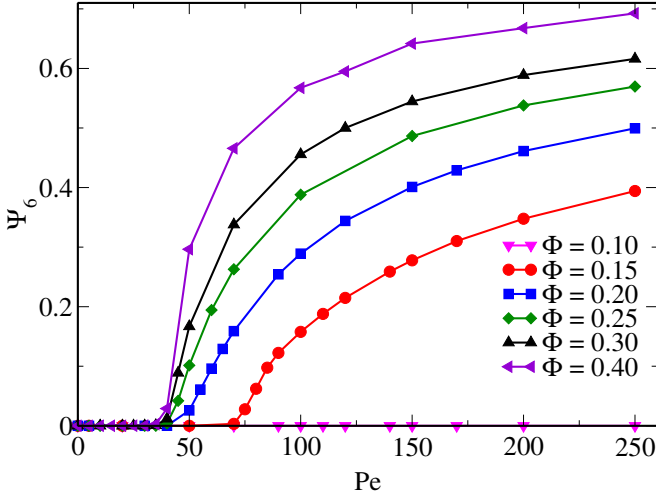


FIG. 3: The average value of Ψ_6 as a function Péclet number plotted for various Φ . The Ψ_6 plot shows a steady increase with Pe after the transition point indicating the growth of crystalline order within the clustered phase.

density profile beyond a transition Péclet number termed here onward as Pe_c .

The distribution $P(\Phi_l)$ suggests that beyond the transition point, the system also consists of a dense aggregate, which we call the largest cluster (N_C). The growth of the clustered phase is quantified using $N_C = \langle \max\{N_S\} \rangle$, where N_S is the size of any cluster in the simulation box. Fig. 2-b illustrates N_C/N as a function of Pe for a range of $\Phi = 0.15$ to 0.4 . The presence of a prominent dense clustered phase results in a sharp transition in the largest cluster size and its size tends to saturate in the limit of high Pe far beyond the transition point.

B. Structure of Cluster

A hexagonal crystalline order is prevalent in the dense clustered phase beyond Pe_c . To corroborate our claim of hexagonal ordering in the largest cluster in 2D, we employ a bond orientational order parameter frequently used in the literature, [36, 72–75],

$$q_6(i) = \frac{1}{6} \sum_{j \in n(i)} e^{i6\theta_{ij}}, \quad (4)$$

where $n(i)$ is the set of six nearest neighbors of i^{th} particle and θ_{ij} is the bond angle between a pair ij around an arbitrary axis. From the local defined parameter q_6 , we derive a global order parameter [36],

$$\Psi_6 = \left\langle \left| \frac{1}{N} \sum_{i=1}^N q_6(i) \right|^2 \right\rangle. \quad (5)$$

The global order parameter Ψ_6 lies in the range of $[0, 1]$, where 0 represents the isotropic phase of the system, 1

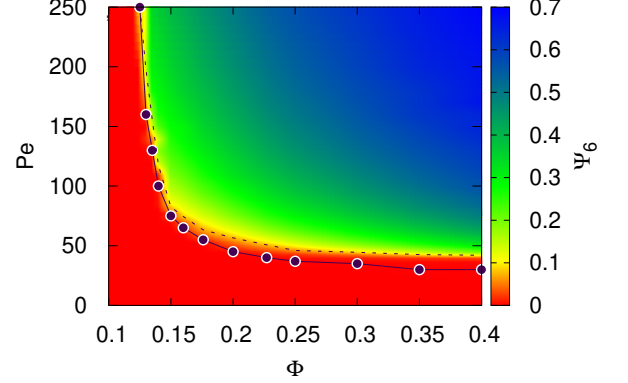


FIG. 4: Phase diagram of the aggregation of active colloids in the presence of quorum-sensing in the parameter space of Pe and Φ . The solid line represents transition point (Pe_c) for phase separation at each Φ determined from the local density distributions. The dashed line highlighted by a thin yellow region in the color map represents the emergence of crystalline ordering within the system ($\Psi_6 \geq 0.1$).

is for the perfect crystalline phase, and the intermediate value corresponds to a fraction of region with hexagonal ordering [36, 72–75]. The order parameter Ψ_6 in the considered system of quorum sensing ABPs is vanishing in the limit of small Péclet numbers ($Pe < Pe_c$). In the phase-separated state, a non-zero value of Ψ_6 appears with a sharp monotonic rise as depicted in Fig. 3. This reveals the presence of a long-range ordered structure. As expected, the degree of ordering increases as a function of Pe and Φ . Analogous to Ψ_6 , a correlation C_{q_6} , is generally used as a measure of local bond-order parameter to distinguish from local crystalline to homogeneous phase. The distribution also highlights a bimodal peak in the phase-separated states (see Fig. SI-3), which manifest local crystalline ordering.

The phase-diagram of the quorum sensing ABPs are quantified and presented in Fig. 4 in the parameter space of Pe and Φ . The solid line in Fig. 4 indicates the transition Péclet number, (Pe_c), for which the local density distribution (Fig 2-b) reveals a bimodal curve. The phase diagram is mapped using values of Ψ_6 corresponding to the color bar in Fig. 4. A homogeneous state is represented by the predominantly red region below the solid line, while the green and blue regions represent the aggregate phase. A thin yellow region illustrates the initiation of hexagonal ordering within the dense clustered phase (also shown by a dashed line in Fig. 4). The narrow region between the phase boundary and the dashed line marks the phase, where the aggregates are formed as a result of phase separation but do not have a significant hexagonal ordering. The Ψ_6 values in this region is negligible compared to the ordered phase. The aggregate attains hexagonal ordering at slightly higher Péclet number. At sufficiently low packing fraction, i.e.,

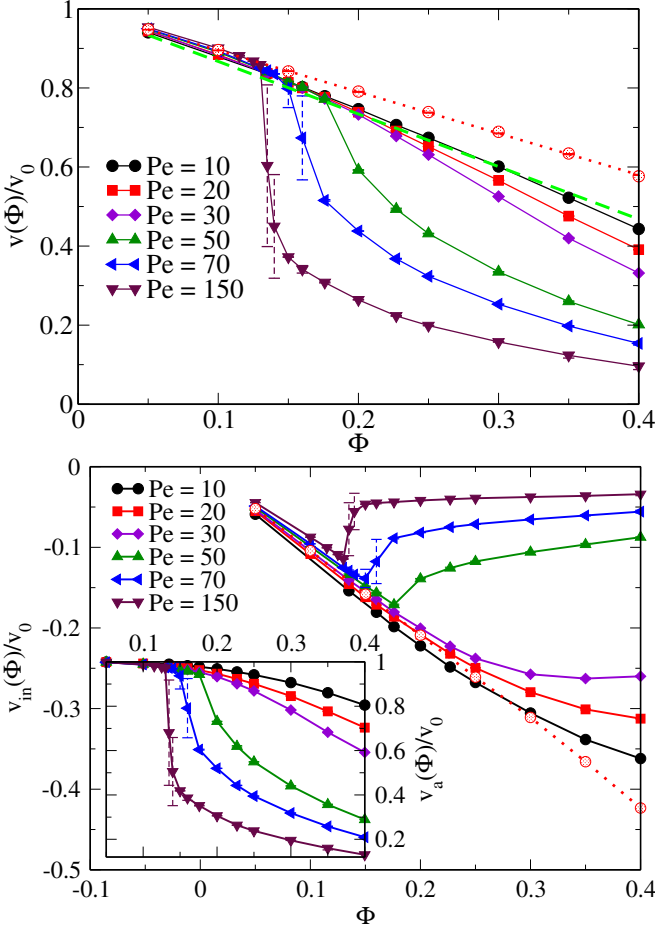


FIG. 5: a) The normalized swim speed as function of packing fraction Φ for various Pe . The dashed line represents a linear fit as $v(\Phi)/v_0 = (1 - a_q\Phi)$ with $a_q = 1.34$ for $Pe = 10$. The plot with red open circle indicates the total swim speed for generic ABPs model $Pe = 30$ [1, 17]. The red dotted line shows the linear fit as $v(\Phi)/v_0 = (1 - a_0\Phi)$ with $a_0 = 1.05$. b) Individual component of the swim speed, interaction term $v_{in}(\Phi)/v_0$ and the active term $v_a(\Phi)/v_0$, are shown in main and inset with Φ for the same set of Pe . The red dotted line corresponds for interaction contribution for generic ABPs model at $Pe = 30$. The active contribution remains constant for such systems.

$\Phi < 0.125$, the system remains homogeneous for all Pe in the simulated window. The transition Péclet number Pe_c decreases rapidly with Φ and saturates at higher values, as displayed from the solid line with bullets in Fig. 4.

C. Swim Speed

The inherent mechanism of MIPS, without attractive or alignment interactions, involves the local slow-down of individual colloids due to an increase in local density. The local inhomogeneity near the transition point is apparent from local density distribution in Fig. 2- a. The existing continuum theoretical models for MIPS is mostly

based on swim speed as an input parameter; therefore, it is crucial to obtain this quantity from the microscopic approach [17, 76]. The numerical values of $v(\Phi)$ can be directly accessed from the simulations. The expression of $v(\Phi)$ is given by,

$$v(\Phi) = \frac{1}{\gamma} \left\langle \left(F'_{a,i} \hat{\mathbf{e}}_i - \sum_{j=1}^{N_m} \nabla_i U_{LJ}(r_{ij}) \right) \cdot \hat{\mathbf{e}}_i \right\rangle. \quad (6)$$

The above expression can also be written as $v = v_a + v_{in}$, where the first term is from the self-propulsive force (v_a), and the second term (v_{in}) is the contribution from the interactions, which in general is negative for repulsive potentials. Additionally, the self-propulsion force itself is a function of local density unlike the generic ABP models where it remains a constant value [17, 76]. In the dilute limit ($\Phi \rightarrow 0$), the interaction contribution vanishes, and the active contribution is nearly unchanged thus $v \rightarrow v_0$, where $v_0 = F_a/\gamma$ is the swim speed of an active colloids in dilute limit.

For the case of low Pe regime, the directed speed follows approximately a linear decay with Φ (see Fig. 5- a), which is in congruence with the previous observations in MIPS in ABPs [17, 76, 77]. The linear behavior of $v(\Phi)$ weakly deviates even in the single-phase at packing reasonably close to the transition point even for small Pe . Notably, the deviations from linearity attain a sharp jump with a non-linear decline in the phase-separated state as displayed in Fig. 5- a for $Pe > Pe_c = 45$. A noteworthy point at small Φ and Pe is that all the curves follow a universal behavior with linear variation.

It is indispensable to analyse the role of active contribution ($v_a(\Phi)$) and the interaction contribution ($v_{in}(\Phi)$) to the swim speed separately to gain further insight. Fig. 5-b shows that the magnitude of the normalised interaction term $v_{in}(\Phi)$ increases linearly with Φ for low Pe . The linear behaviour of $v_{in}(\Phi)$ even in homogeneous phase is likewise of generic ABP models at low Pe . However, the linearity deviates at higher densities even for low Pe in the homogeneous phase. For large $Pe > Pe_c$, $v_{in}(\Phi)/v_0$ sharply decreases with a non-monotonic behavior. Additionally, the inset of Fig. 5- b displays the normalised active contribution, $v_a(\Phi)/v_0$. Here, all curves follow a universal decreases at low densities. The deviation from this universal behavior appears at small Pe , for high densities, even for $Pe = 10$. The deviation displayed for $Pe \geq 20$ is congruent with the behavior of $v(\Phi)$ in Fig. 5- a. Moreover, near the phase-separation ($Pe > Pe_c$), $v_a(\Phi)$ also consist a sharp drop similar to $v(\Phi)$ Fig. 5-a. It reveals that a drastic change in v_a is predominately responsible for the sharp decrease in the directed speed $v(\Phi)$ at larger Pe . Here, the range of quorum-sensing $R_c = 1.3\sigma$ is larger than the short-range LJ interaction. This causes the speed to sharply decrease even before they undergo direct pair-wise collision. Thereby, as expected the slow moving particles will have smaller interaction values of v_{in} to that of fast moving particles. Accordingly, the impact of collision con-

tribution becomes weaker, hence v_{in} for denser system sharply diminishes which is captured in Fig. 5-b main plot, at $Pe = 50, 70$, and 150).

Furthermore, we have computed local swim speed with local packing fraction Φ_l , which is illustrated in Fig. SI-6. The behavior is very similar to the globally averaged quantity, which additionally corroborates the claim of local slow-down at the microscopic level. To summarise, multi-body collisions emerges at higher Pe and Φ , causing to set in the quorum-sensing behavior, which plays dominant role in the reduction of the directed speed unlike the generic ABP model where interaction term is vital.

D. Dynamics of cluster

The dynamical behavior of a colloid in the aggregate can be assessed through its mean-square-displacement (MSD). At the boundary of the aggregate, the colloid moves in and out from the cluster. Therefore, a convenient way to compute the MSD of the clustered particles is to consider those particles which are close to the centre of the cluster so that they do not leave the cluster in the characterised time window. As expected, at short time scales, the particles exhibit sub-diffusive behavior due to the constraint from the presence of several neighboring colloids in its proximity (see Fig. 6-a). At intermediate time scale, the self-propulsion is suppressed as the particles are caged within the aggregate. Consequently, MSD attains a plateau at this timescale. More importantly, the width of the plateau widens and becomes more prominent at higher Pe , as Fig. 6-a illustrates for a range of $Pe = 70$ to 200 . In the long time limit, colloid attains diffusive behavior. The enhanced diffusive dynamics of colloids are evident from MSD curves in the timescale $t > 0.1\tau$. A dashed line indicates the super-diffusive behavior, where the MSD is super-diffusive according to $\langle \Delta r^2(t) \rangle \sim t^{3/2}$ with an exponent $3/2$. The super-diffusive behavior is a consequence of large active force on the surface of the cluster, which drives significant fluctuations in its shape and additionally the propagation of fast-moving defects inside the cluster. The defect dynamics and shape of the cluster is illustrated in SI-Movie-1 and 2 for visualisation.

The characteristic dynamical features of the colloids can be presented in terms of the effective diffusion coefficient. For this, the MSD of the colloids is averaged over all particles (Fig. SI-4). The measured effective diffusion coefficient, from the diffusive regime, is plotted as a function of Pe in Fig. 6-b. For $\Phi = 0.05$, the effective diffusion coefficient increases quadratically with Pe . On contrary, for $\Phi \geq 0.125$ and $Pe > Pe_c$, D_τ grows with a power of exponent $3/2$ with Pe (see Fig. 6-b). The effective diffusion coefficient shows a cross-over from Pe^2 quadratic growth in the homogeneous state to $Pe^{3/2}$ behavior in the phase-separated state.

The inset of Fig.6-b shows behavior of the normalised

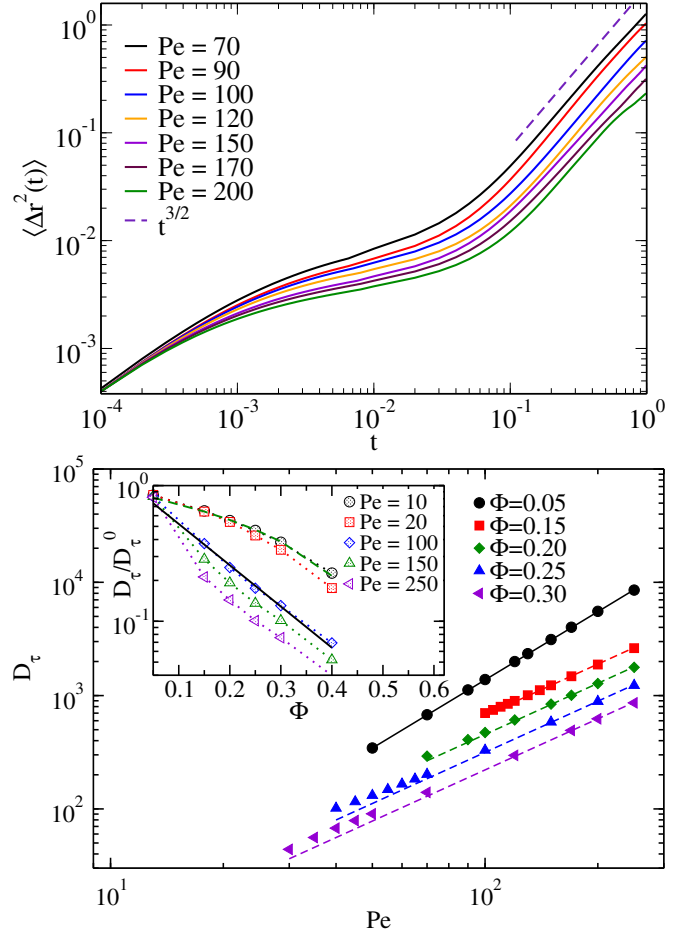


FIG. 6: a) The MSD of particles deep inside the cluster for different Pe . The dashed line shows the super-diffusive behavior as $t^{3/2}$. b) The effective diffusion coefficient as a function of Péclet number for $\Phi = 0.05$ to $\Phi = 0.4$. The solid line shows power-law behavior, $D_\tau \approx Pe^2$, and dashed lines as $D_\tau \approx Pe^{3/2}$. The inset shows normalized D_τ/D_τ^0 as a function of Φ for various Pe . The solid line displays exponential fit as $D_\tau/D_\tau^0 \sim e^{-b_2\Phi}$, with $b_2 \approx 7.0$, while the dashed line displays linear fit as $D_\tau/D_\tau^0 \sim 1 - b_1\Phi$ with $b_1 = 1.9$.

D_τ/D_τ^0 , where $D_\tau^0 = D_t(1 + \frac{1}{6}Pe^2)$ is the effective diffusion coefficient for ideal active particles at the same Pe [18, 19]. As expected from the effective diffusion coefficient, the diffusive dynamics of particle substantially slows down with Φ , as D_τ decreases with Φ for all Pe [18]. In the homogeneous phase, the effective diffusion coefficient follows approximately a linear behaviour, $D_\tau(\Phi)/D_\tau^0 \sim 1 - b_1\Phi$ with $b_1 \approx 1.9$ with a larger slope reported in previous studies [17, 76, 77]. However, for $Pe > Pe_c$, the diffusion is suppressed sharply, as result shows an exponential behavior as, $D_\tau(\Phi)/D_\tau^0 \sim \exp(-b_2\Phi)$ with $b_2 \approx 7.0$.

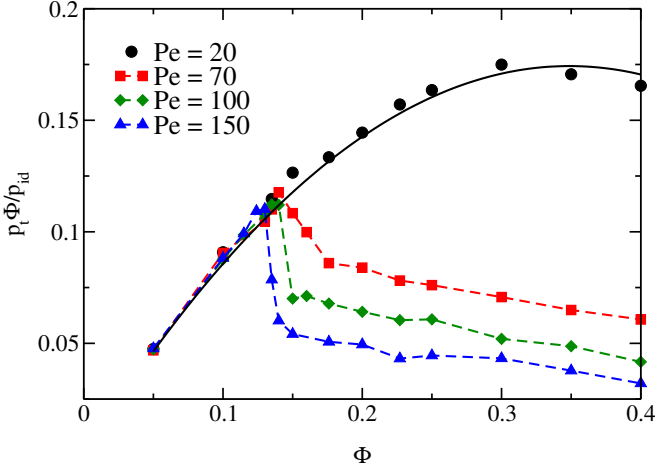


FIG. 7: Total pressure p_t plotted as a function of Φ for various $Pe = 20, 70, 100$ and 150 . Solid line shows the function, $p_t = \phi(1 - \kappa\Phi)$, where $\kappa \approx 1.42$.

E. Pressure

The total pressure of a system undergoing MIPS is used to identify phase boundaries as it exhibits a non-monotonic behavior on the density with a sharp jump at the transition point [18, 49]. The total pressure exhibits contributions from the thermal fluctuations, the interaction force, and the active force (active pressure). Total pressure can be expressed as $p_t = p_0 + p_a + p_{in}$, with individual contributions as, $p_0 = k_B T/A$, the ideal gas pressure in 2D, p_a , the active pressure, and p_{in} , the standard virial term due to inter-particle interactions. The explicit forms of p_a and p_{in} are given as,

$$p_a = \frac{\gamma}{2AN} \sum_i^N \langle \mathbf{F}'_{a,i} \cdot \hat{\mathbf{e}}_i \cdot \mathbf{r}_i \rangle,$$

$$p_{in} = \frac{1}{4AN} \sum_{j,i}^N \langle \mathbf{F}_{ij} \cdot (\mathbf{r}_i - \mathbf{r}_j) \rangle. \quad (7)$$

The total pressure $p_t(\Phi)$ defines an equation of state of ABPs without confinement. The ideal swim pressure is given as $p_{id}A = k_B T(1 + \frac{1}{6}Pe^2)$ at a temperature T in two dimensions [18, 19]. This expression acts as pressure for the ideal active particles at any density.

Figure 7 presents the scaled total pressure with p_{id} multiplied by Φ . Importantly, $p_t\Phi/p_{id}$ shows a universal behavior until the onset of phase separation. In the single-phase, we can write pressure as $p_t\Phi/p_{id} = \Phi(1 - \kappa\Phi)$ with $\kappa = 1.42$. A sudden drop in pressure occurs at the transition point [18, 20, 78] in Fig. 7. It suggests a discontinuous drop in active particles' pressure due to slowdown of their speed in clusters. This behavior is in contrast to the plot of a continuous parabolic profile for $Pe = 20$, where system exist in a homogeneous single phase. The change in the behavior of pressure in the

TABLE I: Values of α , β , and strength of active force F'_{a6}/F_a at $\Phi = 0.2$. Here $F'_a = F'_{a6}$ corresponds to the values of active force for $n \geq 6$.

α	β	F'_a/F_a
1.0	1.8	0.0
1.06	1.62	0.1
1.14	1.44	0.2
1.24	1.26	0.3
1.37	1.08	0.4
1.55	0.8	0.5

phase-separated state is a consequence of large-number fluctuations in the active systems [17] (see Fig. SI-1). It is important to emphasize here that relatively more pronounced drop in pressure is noticeable at the transition point than the previous studies [18, 20, 78]. In phase separated state, active contribution dominates (see Fig. SI-5), which shows that the surface effects are more prominent in the behavior of global variables.

F. Non-vanishing Motility of Quorum-Sensing

All the results so far discussed corresponds to the particular case where the active force becomes zero whenever a colloid gets surrounded by six or more colloids as defined in Eq. 3. Now we test our approach to a broader class of problem by mimicking non-zero motility in the dense region for $n \geq 6$. The mathematical equation for the density-dependent motility is same as given in Eq. 3, while the choice of α and β dictates a non-zero active force at $n \geq 6$, and are listed in table I. A series of simulations are carried out for a range of F'_{a6}/F_a , where F_{a6} is the active force at $n \geq 6$, to test its influence on the phase-separation and robustness of the choice of the approach. The summary of results are translated into a phase diagram in Fig. 8, where it displays the aggregation of colloids in the parameter space of Pe and ratio of F'_{a6}/F_a at $\Phi = 0.2$. The shaded area in the plot displays phase separated state with hexagonal ordering. It indicates that the system continues to retain phase separation up to $F'_{a6}/F_a \leq 0.3$. As expected, phase-separation disappears for larger residual motility, and system attains the homogeneous phase further for $\Phi = 0.2$.

IV. SUMMARY

We have presented over-damped Langevin dynamics simulations of active colloids whose motility vary with their local density. The alteration of self-propulsion speed with density is observed in nature for example bacterial systems [79]. A local model of quorum-sensing has been adopted in the past for the study of collective phenomena in active systems, and it displays fascinating global dynamics [70, 71, 80, 81]. Our study reports that

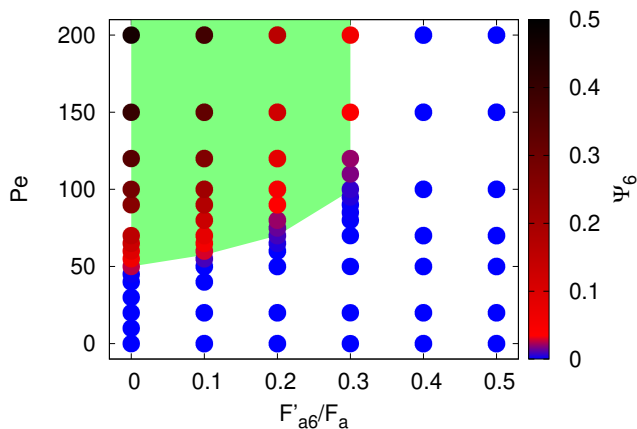


FIG. 8: Phase diagram of the aggregation of active colloids in the presence of quorum-sensing in the parameter space of Pe and F'_{a6}/F_a at $\Phi = 0.2$.

the system phase separates into a dense phase coexisting with a low-density phase at very small packing fractions ($\Phi \geq 0.125$) [11, 36, 46]. The dense clustered phase acquires hexatic ordering at higher activity strength beyond the critical point. Active particles in the cluster exhibit sub-diffusive dynamics at a short time due to local caging from neighboring particles. The effective diffusion coefficient grows according to $Pe^{3/2}$ in the phase-separated state, [18, 20] while a parabolic increase in the homogeneous phase is reported.

It has previously been established that MIPS is a consequence of a positive feedback mechanism between accumulation induced slow down, and slow speed drives accumulation in ABP models [54, 82]. In our study, the mechanism behind aggregation is instigated by quorum-sensing phenomenon due to emergence of multi-body collisions at higher density and Pe . This sets up an apparent slow-down causes a sharp decline in the relative directed speed. Further, we have revealed that the slow down is dominated by quorum-sensing contribution (see Fig.5-b). Notably, the role of interaction contribution is weaker in contrast to the generic models. Slow down of speed also accounts for the reduction in effective-diffusivity, facilitating a crossover from the linear to exponential behavior.

The phase-separation strongly depends on the choice of the R_c , a larger R_c will push the phase-separation at slower self-propulsion speeds or smaller packing fractions. A smaller values will lead our model towards the standard

ABP model, and the phase-separation at lower packing disappears. Additionally, it can also be visualized in simulations that the density-dependent contribution is sufficient enough to bring the phase-separation, likewise in the theoretical studies [78], at relatively small Péclet numbers. Besides, these phase-separated states lag the long-range ordering present in largest cluster without pair-wise repulsive force (see Figure SI-7).

The linear behavior of $v(\Phi)$ and $D(\Phi)$ in single phase with existing models [17, 78] exhibits the coefficients $a_q = 1.34$ and $b_1 = 1.9$ larger than the previously reported approach [17, 54, 82]. The Eq.3 suggests quorum-sensing influence causes a bigger effective diameter of colloidal interaction ($R_c = 1.3$) than the generic repulsive ABP models, consequently they exhibit a larger effective scattering cross-section. This attributes to steeper slope (a_q and b_1) in the reduction of directed speed and effective diffusion coefficient.

The presented results are not unique for the adopted linear model proposed in Eq. 3; an exponentially decaying self-propulsion force also yields a similar phase-separation nearly at the same packing fraction. The qualitative behavior is presented in the supplementary text; see Fig. SI-7, and 8. In conclusion, a microscopic model of local density-dependent motility plays a crucial role in the kinetics of MIPS at low density, and the same mechanism also facilitates phase separation. The reduction in local directed speed (see SI-Fig. 6) of colloids asserts the importance of probing the microscopic dynamics, it may be useful in providing a complete picture of phase-diagram. Our approach considers simpler interactions; however various other effects may play a vital role in the collective dynamics. For example, viscous lubrication, hydrodynamics, and anisotropic shape of colloids may be worth considering for the realistic models. Additionally, a model of coarse-grained density (where local density is computed in weighted averaged fashion) over microscopic model might serve a better purpose in direct comparison with theoretical results [57].

Acknowledgements

The authors would like to thank the HPC facility at IISER Bhopal for the computation time and DST SERB Grant No. YSS/2015/000230 and CRG/2020/000661 for the financial support. SKA and FJ thank Harsh Kumar for indulging in useful discussions at the initial stage of the work.

-
- [1] M. C. Marchetti, J.-F. Joanny, S. Ramaswamy, T. B. Liverpool, J. Prost, M. Rao and R. A. Simha, *Reviews of Modern Physics*, 2013, **85**, 1143.
 - [2] M. E. Cates, *Reports on Progress in Physics*, 2012, **75**, 042601.

- [3] A. Zöttl and H. Stark, *Journal of Physics: Condensed Matter*, 2016, **28**, 253001.
- [4] L. Corte, P. M. Chaikin, J. P. Gollub and D. J. Pine, *Nature Physics*, 2008, **4**, 420.
- [5] F. Peruani, A. Deutsch and M. Bär, *Physical Review E*,

- 2006, **74**, 030904.
- [6] A. Gopinath, M. F. Hagan, M. C. Marchetti and A. Baskaran, *Physical Review E*, 2012, **85**, 061903.
 - [7] O. Pohl and H. Stark, *Physical review letters*, 2014, **112**, 238303.
 - [8] Z. Lin, C. Gao, M. Chen, X. Lin and Q. He, *Current opinion in colloid & interface science*, 2018, **35**, 51–58.
 - [9] V. Narayan, S. Ramaswamy and N. Menon, *Science*, 2007, **317**, 105–108.
 - [10] H. Chaté, F. Ginelli and R. Montagne, *Phys. Rev. Lett.*, 2006, **96**, 180602.
 - [11] G. S. Redner, A. Baskaran and M. F. Hagan, *Phys. Rev. E*, 2013, **88**, 012305.
 - [12] T. Mora, A. M. Walczak, L. Del Castello, F. Ginelli, S. Melillo, L. Parisi, M. Viale, A. Cavagna and I. Giardina, *Nature physics*, 2016, **12**, 1153–1157.
 - [13] M. Ballerini, N. Cabibbo, R. Candelier, A. Cavagna, E. Ciliberto, I. Giardina, V. Lecomte, A. Orlandi, G. Parisi, A. Procaccini *et al.*, *Proceedings of the national academy of sciences*, 2008, **105**, 1232–1237.
 - [14] A. Cavagna, D. Conti, C. Creato, L. Del Castello, I. Giardina, T. S. Grigera, S. Melillo, L. Parisi and M. Viale, *Nature Physics*, 2017, **13**, 914–918.
 - [15] A. Bricard, J.-B. Caussin, D. Das, C. Savoie, V. Chikkadi, K. Shitara, O. Chepizhko, F. Peruani, D. Saintillan and D. Bartolo, *Nature communications*, 2015, **6**, 1–8.
 - [16] J. Yan, M. Han, J. Zhang, C. Xu, E. Luijten and S. Granick, *Nature materials*, 2016, **15**, 1095.
 - [17] Y. Fily and M. C. Marchetti, *Physical review letters*, 2012, **108**, 235702.
 - [18] R. G. Winkler, A. Wysocki and G. Gompper, *Soft matter*, 2015, **11**, 6680–6691.
 - [19] A. P. Solon, J. Stenhammar, R. Wittkowski, M. Kardar, Y. Kafri, M. E. Cates and J. Tailleur, *Phys. Rev. Lett.*, 2015, **114**, 198301.
 - [20] S. C. Takatori, W. Yan and J. F. Brady, *Phys. Rev. Lett.*, 2014, **113**, 028103.
 - [21] J. Palacci, S. Sacanna, A. P. Steinberg, D. J. Pine and P. M. Chaikin, *Science*, 2013, **339**, 936–940.
 - [22] D. P. Singh, U. Choudhury, P. Fischer and A. G. Mark, *Advanced Materials*, 2017, **29**, 1701328.
 - [23] I. Buttinoni, J. Bialké, F. Kümmel, H. Löwen, C. Bechinger and T. Speck, *Physical review letters*, 2013, **110**, 238301.
 - [24] I. Buttinoni, G. Volpe, F. Kümmel, G. Volpe and C. Bechinger, *Journal of Physics: Condensed Matter*, 2012, **24**, 284129.
 - [25] F. Ginot, I. Theurkauff, F. Detcheverry, C. Ybert and C. Cottin-Bizonne, *Nature communications*, 2018, **9**, 696.
 - [26] I. Theurkauff, C. Cottin-Bizonne, J. Palacci, C. Ybert and L. Bocquet, *Physical review letters*, 2012, **108**, 268303.
 - [27] J. Palacci, S. Sacanna, S.-H. Kim, G.-R. Yi, D. Pine and P. Chaikin, *Philosophical Transactions of the Royal Society A: Mathematical, Physical and Engineering Sciences*, 2014, **372**, 20130372.
 - [28] F. Schmidt, B. Liebchen, H. Löwen and G. Volpe, *The Journal of chemical physics*, 2019, **150**, 094905.
 - [29] M. Lee, K. Szuttor and C. Holm, *The Journal of chemical physics*, 2019, **150**, 174111.
 - [30] H. C. Berg and D. A. Brown, *Nature*, 1972, **239**, 500–504.
 - [31] L. Turner, W. S. Ryu and H. C. Berg, *Journal of bacteriology*, 2000, **182**, 2793–2801.
 - [32] G. Ariel, M. Sidortsov, S. D. Ryan, S. Heidenreich, M. Bär and A. Be’er, *Physical Review E*, 2018, **98**, 032415.
 - [33] M. Paoluzzi, C. Maggi, U. M. B. Marconi and N. Gnan, *Physical Review E*, 2016, **94**, 052602.
 - [34] C. Maggi, M. Paoluzzi, A. Crisanti, E. Zaccarelli and N. Gnan, *arXiv preprint arXiv:2007.12660*, 2020.
 - [35] L. Caprini, E. Hernández-García, C. López and U. M. B. Marconi, *Scientific reports*, 2019, **9**, 1–13.
 - [36] J. Bialké, T. Speck and H. Löwen, *Physical review letters*, 2012, **108**, 168301.
 - [37] T. Speck, J. Bialké, A. M. Menzel and H. Löwen, *Physical Review Letters*, 2014, **112**, 218304.
 - [38] T. Speck, A. M. Menzel, J. Bialké and H. Löwen, *The Journal of chemical physics*, 2015, **142**, 224109.
 - [39] J. Bialké, H. Löwen and T. Speck, *EPL (Europhysics Letters)*, 2013, **103**, 30008.
 - [40] M. Pu, H. Jiang and Z. Hou, *Soft Matter*, 2017, **13**, 4112–4121.
 - [41] M. E. Cates, D. Marenduzzo, I. Pagonabarraga and J. Tailleur, *Proceedings of the National Academy of Sciences*, 2010, **107**, 11715–11720.
 - [42] S. R. McCandlish, A. Baskaran and M. F. Hagan, *Soft Matter*, 2012, **8**, 2527–2534.
 - [43] G. S. Redner, M. F. Hagan and A. Baskaran, *Physical review letters*, 2013, **110**, 055701.
 - [44] S. K. Anand and S. P. Singh, *Physical Review E*, 2018, **98**, 042501.
 - [45] S. K. Anand and S. P. Singh, *Physical Review E*, 2020, **101**, 030501.
 - [46] J. Bialké, T. Speck and H. Löwen, *Journal of Non-Crystalline Solids*, 2015, **407**, 367–375.
 - [47] M. E. Cates and J. Tailleur, *Annu. Rev. Condens. Matter Phys.*, 2015, **6**, 219–244.
 - [48] M. E. Cates and J. Tailleur, *EPL (Europhysics Letters)*, 2013, **101**, 20010.
 - [49] P. Digregorio, D. Levis, A. Suma, L. F. Cugliandolo, G. Gonnella and I. Pagonabarraga, *Physical review letters*, 2018, **121**, 098003.
 - [50] G. Gonnella, D. Marenduzzo, A. Suma and A. Tiribocchi, *Comptes Rendus Physique*, 2015, **16**, 316–331.
 - [51] J. Barré, R. Chétrite, M. Muratori and F. Peruani, *Journal of Statistical Physics*, 2015, **158**, 589–600.
 - [52] A. Suma, G. Gonnella, D. Marenduzzo and E. Orlandini, *EPL (Europhysics Letters)*, 2014, **108**, 56004.
 - [53] E. Sese-Sansa, I. Pagonabarraga and D. Levis, *EPL (Europhysics Letters)*, 2018, **124**, 30004.
 - [54] M. E. Cates and J. Tailleur, *EPL (Europhysics Letters)*, 2013, **101**, 20010.
 - [55] P. Digregorio, D. Levis, A. Suma, L. F. Cugliandolo, G. Gonnella and I. Pagonabarraga, *Phys. Rev. Lett.*, 2018, **121**, 098003.
 - [56] L. Caprini, U. M. B. Marconi and A. Puglisi, *Physical Review Letters*, 2020, **124**, 078001.
 - [57] A. P. Solon, J. Stenhammar, M. E. Cates, Y. Kafri and J. Tailleur, *Physical Review E*, 2018, **97**, 020602.
 - [58] A. Patch, D. Yllanes and M. C. Marchetti, *Physical Review E*, 2017, **95**, 012601.
 - [59] J. Agudo-Canalejo and R. Golestanian, *Physical review letters*, 2019, **123**, 018101.
 - [60] K. Ishimoto and E. A. Gaffney, *Scientific reports*, 2018, **8**, 15600.
 - [61] G. Reid, A. W. Bruce, M. Llano, J. McGroarty and M. Blake, *Current Microbiology*, 1990, **20**, 185–190.

- [62] F. D. Schramm, K. Schroeder and K. Jonas, *FEMS Microbiology Reviews*, 2020, **44**, 54–72.
- [63] C. Fuqua, S. C. Winans and E. P. Greenberg, *Annual review of microbiology*, 1996, **50**, 727–751.
- [64] S. P. Brown and R. A. Johnstone, *Proceedings of the Royal Society of London. Series B: Biological Sciences*, 2001, **268**, 961–965.
- [65] C. Lupp and E. G. Ruby, *Journal of bacteriology*, 2005, **187**, 3620–3629.
- [66] V. Sperandio, A. G. Torres and J. B. Kaper, *Molecular microbiology*, 2002, **43**, 809–821.
- [67] B. L. Bassler, *Current opinion in microbiology*, 1999, **2**, 582–587.
- [68] B. J. Crespi, *Trends in ecology & evolution*, 2001, **16**, 178–183.
- [69] T. Bäuerle, A. Fischer, T. Speck and C. Bechinger, *Nature communications*, 2018, **9**, 1–8.
- [70] C. A. Velasco, M. Abkenar, G. Gompper and T. Auth, *Physical Review E*, 2018, **98**, 022605.
- [71] F. Farrell, M. Marchetti, D. Marenduzzo and J. Tailleur, *Physical review letters*, 2012, **108**, 248101.
- [72] M. Theers, E. Westphal, K. Qi, R. G. Winkler and G. Gompper, *Soft matter*, 2018, **14**, 8590–8603.
- [73] A. Zöttl and H. Stark, *Physical review letters*, 2014, **112**, 118101.
- [74] P. J. Steinhardt, D. R. Nelson and M. Ronchetti, *Physical Review B*, 1983, **28**, 784.
- [75] C. Tung, J. Harder, C. Valeriani and A. Cacciuto, *Soft Matter*, 2016, **12**, 555–561.
- [76] J. Stenhammar, A. Tiribocchi, R. J. Allen, D. Marenduzzo and M. E. Cates, *Physical review letters*, 2013, **111**, 145702.
- [77] J. Stenhammar, D. Marenduzzo, R. J. Allen and M. E. Cates, *Soft matter*, 2014, **10**, 1489–1499.
- [78] A. P. Solon, H. Chaté and J. Tailleur, *Physical review letters*, 2015, **114**, 068101.
- [79] A. Sokolov, I. S. Aranson, J. O. Kessler and R. E. Goldstein, *Phys. Rev. Lett.*, 2007, **98**, 158102.
- [80] S. Mishra, K. Tunstrøm, I. D. Couzin and C. Huepe, *Physical Review E*, 2012, **86**, 011901.
- [81] A. Fischer, F. Schmid and T. Speck, *Physical Review E*, 2020, **101**, 012601.
- [82] J. Tailleur and M. Cates, *Physical review letters*, 2008, **100**, 218103.